lubricants

Review

A Review of In-Situ TEM Studies on the Mechanical and Tribological Behaviors of Carbon-Based Materials

Zelong Hu, Xue Fan * and Dongfeng Diao

Guangdong Provincial Key Laboratory of Micro/Nano Optomechatronics Engineering, Institute of Nanosurface Science and Engineering, College of Mechatronics and Control Engineering, Shenzhen University, Shenzhen 518060, China
* Correspondence: fanx@szu.edu.cn

Abstract: Carbon-based materials are widely applied in various devices due to their outstanding mechanical and tribological behaviors. In recent years, more attention has been paid to clarifying the nanocontact mechanisms of carbon-based materials, in order to promote nanoscale applications. The in-situ TEM method is currently the only way that can combine contact behavior and real interface. However, there is still a lack of a systematic summary of in-situ TEM studies on carbon-based materials. Therefore, this work provides an overview of in-situ TEM mechanical and tribological studies on carbon-based materials, consisting of the quantitative actuation and detection for in-situ tests, the strength of fracture and yield, the adhesion between interfaces, the friction performance, and wear features of carbon-based materials with different nanostructures, such as carbon nanotube, graphene, graphite, amorphous, sp^2 nanocrystalline, and ultrananocrystalline diamond. Nanostructures play a crucial role in determining mechanical and tribological behaviors. Perspectives on current challenges and future directions are presented, with the aim of promoting the advancement of in-situ TEM research.

Keywords: in-situ TEM; carbon-based materials; mechanics; tribology

Citation: Hu, Z.; Fan, X.; Diao, D. A Review of In-Situ TEM Studies on the Mechanical and Tribological Behaviors of Carbon-Based Materials. *Lubricants* **2023**, *11*, 187. https://doi.org/10.3390/lubricants11050187

Received: 2 April 2023
Revised: 19 April 2023
Accepted: 21 April 2023
Published: 24 April 2023

1. Introduction

Carbon-based materials exhibit outstanding mechanical and tribological behaviors owing to their various allotropes. Simple nanostructures such as carbon nanotubes (CNT) and graphene demonstrate high strength [1,2], while carbon films with complex nanostructures show diverse friction behaviors [3,4]. The run-in period of amorphous carbon (*a-C*) films can be dramatically shortened by a graphene nanocrystallite cap layer, which can restructure quickly on the sliding interface [5]. The sp^2 nanocrystallited carbon films show a low friction coefficient and minimal wear at multi-scales due to their considerable hardness resulting in a smaller real-contact area [6]. Carbon films with a loosely exploded graphene nanocrystallite structure, fabricated by direct laser writing on polyimides, show ultra-wear-resistance due to the formation of a tough cross-linked nanocrystalline transfer film on the sliding interface [7]. Overall, the various mechanical and tribological behaviors of carbon-based materials are attributed to their different nanostructures.

In recent years, more attention has been paid to clarifying the nanocontact mechanisms of carbon-based materials, in order to promote nanoscale applications, such as nanomanipulations based on the sliding of nanoprobes including nanomaterial characterizations [8], nanosurface adjustments [9], robotic nanomanipulators [10], nanosemiconductor equipment manufacturing [11], and patterned processing of integrated circuits [12]. One major challenge is the surface effects caused by a higher ratio of the superficial area to volume at the micro-/nanoscale [13]. This leads to adhesive plastic deformation and a failure of the contact interface, which can impact the accuracy and reliability of micro-/nano-devices or nanoprocessing methods. To sum up, it is necessary to comprehend and predict the contact and sliding behaviors of carbon-based materials at the nanoscale, with a focus on exploring the contact interface.

Numerous studies have been conducted from different aspects of the contact interface, including the adjustment of friction by surface designing [14], surface passivation [15] or tribo-layer formation [16], the enhancement of adhesion by dynamic sliding [17], and achieving superlubricity by incommensurate contact [18]. Changes in the contact area and contact quality are common characteristics. The contact area can be quantitatively measured through normal/lateral contact stiffness [19,20], and the contact quality can be accurately reflected by the interaction of the interface [21]. However, the formation, evolution, detaching, and transferring processes of the contact interface remain a black box that is invisible and untouchable, and scientific problems related to the atomic bonding structure, contact, adhesion, and friction buried within the interface are entangled. As of now, transmission electron microscopy (TEM) is the only available equipment to observe atomic structures at the nanoscale, which can be exploited to confirm the evolution of wear volume [22] and characterize variations in the nanostructure through direct observation [23]. With the in-situ TEM method, properties of the interface can be measured [24], and the nanostructure of materials can be acquired under different physical fields, such as thermal [25], magnetic [26], electric [27], optical [28], and stress [29] ones, which provides a powerful approach to discovering new phenomena and uncovering novel mechanisms. Exploiting TEM to perform the non-absorbing, pure contact and sliding experiments provides an efficient way to unveil the mask of the sliding interface, which is helpful for understanding, controlling, and utilizing the carbon nanocontact interfaces.

Therefore, this work provides an overview of in-situ TEM studies on the mechanical and tribological behaviors of carbon-based materials with different nanostructures, as shown in Figure 1, which includes three sections of quantitative actuation and detection (Section 2), mechanical properties (Section 3), and tribological behaviors (Section 4). The nanostructures examined in this work include carbon nanotube, graphene, graphite, amorphous, sp^2 nanocrystalline, and ultrananocrystalline diamond.

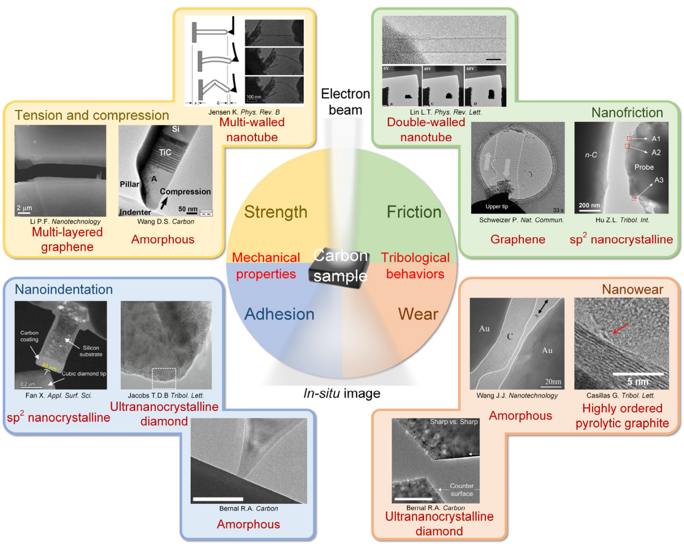

Figure 1. Classification of the in-situ TEM mechanical and tribological studies on carbon-based materials with different nanostructures. The data is from the Web of Science. The criterion of selecting papers concerns the different in-situ TEM tests employed on carbon-based materials with different nanostructures. The dates range from 2007 to the present. Reproduced with permission from Ref. [30]. American Physical Society, 2007; Ref. [31]. IOP Publishing, 2019; Ref. [32]. Elsevier, 2014; Ref. [33]. Elsevier, 2016; Ref. [34]. Springer Nature, 2013; Ref. [35]. Elsevier, 2018; Ref. [36]. American Physical Society, 2011; Ref. [37]. Springer Nature, 2020; Ref. [38]. Elsevier, 2022; Ref. [39]. IOP Publishing, 2009; Ref. [40]. Springer Nature, 2015; and Ref. [41]. Elsevier, 2019.

2. Quantitative Actuation and Detection

In order to clarify the nanocontact mechanism, it is integral to capture normal and lateral force quantitatively during in-situ TEM nanomechanical and nanotribological experiments while observing the dynamic evolution of micro-/nano-deformation. However, the gap between pole pieces of high-resolution TEM is typically small, usually only a few millimeters. Therefore, the development of microelectromechanical system (MEMS) devices is essential to realize in-situ TEM nanomechanical and nanotribological tests. Figure 2 shows a classification of the various MEMS devices used in in-situ TEM mechanical and tribological studies, which can be categorized as sample-separated MEMS and sample-integrated MEMS. Over time, the appearance of double-axial MEMS and the improvement of force-detection accuracy has allowed for the successful clarification of the nanocontact mechanism.

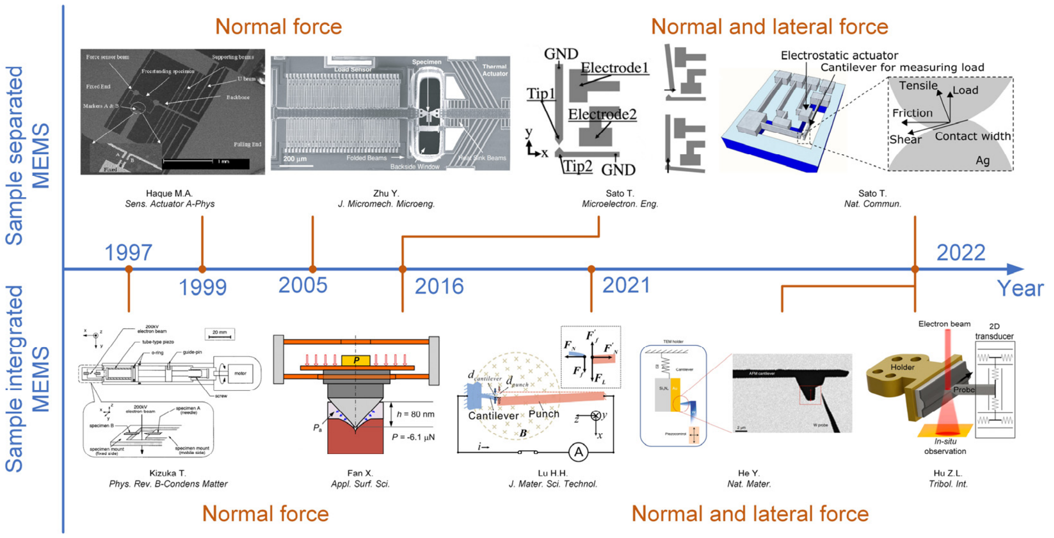

Figure 2. Classification of the various MEMS devices used in in-situ TEM mechanical and tribological studies. The data is from the Web of Science. The selected papers were chosen based on the criterion that the MEMS devices exploited were to detect in-situ forces by different methods. The dates range from the earliest in-situ TEM MEMS devices in 1997 to the present. Timeline shows the appearances of representative MEMS devices, with a focus on test samples being carbon-based materials. Reproduced with permission from Ref. [42]. American Physical Society, 1997; Ref. [43]. Elsevier, 2002; Ref. [44]. IOP Publishing, 2006; Ref. [45]. Elsevier, 2016; Ref. [33]. Elsevier, 2016; Ref. [46]. Elsevier, 2021; Ref. [47]. Springer Nature, 2022; Ref. [48]. Springer Nature, 2022; and Ref. [38]. Elsevier, 2022.

2.1. Sample-Integrated MEMS

Sample-integrated MEMS devices can be exploited to perform in-situ tensile and nanocontact tests, which mainly consist of an actuator and detector, and integrates test samples by either a focused ion beam (FIB) fixation or ion beam etching after direct deposition.

In 1999, Haque et al. [49,50] started to develop a MEMS device used for in-situ tensile observations. In 2002, a MEMS device was put forward, which was mounted on the TEM straining stage for actuation [43,51]. Markers A and B were used to quantitatively reflect the force and displacements, respectively. The tensile mode was force controlled, and a freestanding aluminum specimen with a nanometer thickness was fabricated to confirm the feasibility of the MEMS device. Later, Zhu et al. [52] developed a MEMS device that consisted of a thermal actuator and a capacitive load sensor. One side of the specimen was connected with a rigid shuttle, and the shuttle could be stretched and pushed by thermal expansion. The capacitance change between the two capacitors was proportional to displacement. The response of the MEMS device was optimized, and its performance was examined with a polysilicon freestanding specimen [44]. With various MEMS devices and methods, the one dimensional tensile and compression properties of nanomaterials can be investigated by directly observing their structural variation with strain–stress evolutions.

Besides the uniaxial tensile of one single sample, MEMS devices also can integrate two samples to realize the nanocontact between samples. Ishida et al. [53] designed a MEMS device with an electrostatic actuator and two tips to clarify nanocontact properties. The tips with evaporated gold were sharpened by FIB etching. In addition, the electrostatic actuator drove the movable electrode (one tip) to the fixed electrode (the other tip). The approach-contact-retraction-fracture process between two gold tips was observed successfully with an in-situ TEM test. Afterwards, the MEMS device was improved by adding a new electrode to actuate the tip in the lateral direction, and the nanocontact process of two silicon nanojunctions was successfully observed while detecting the normal force and lateral force in real-time [45]. By exploiting the MEMS actuation and examining the nanoscale real-contact area during the sliding of two silver asperities through an in-situ TEM test, the close relation between the energy loss within a shear fracture event and the increase of total surface energy was clarified [54,55]. By conducting in-situ TEM tests between silicon asperities at an ultralow speed of 0.01 nm/s under high contact stress of the GPa order, the superplastic behavior of silicon was demonstrated, which was induced by decrystallization, plastic deformation, and atomic diffusion at the contact interface [56]. This design of sample and actuator integration was widely used in in-situ TEM tensile and nanocontact experiments [47,57,58]. One major advantage is its ease of realization and ability to avoid positioning and alignment problems. However, sample-integrated MEMS typically require the samples to be machined with ion etching for a significant amount of time, which limits the choice of materials. Additionally, for more complex experimental requirements such as nanoindentation, nanoscratch, and nanowear, sample-integrated MEMS may not be sufficient to achieve the desired functionality.

2.2. Sample-Separated MEMS

One of the main challenges with sample-separated MEMS is the requirement for precise positioning and alignment, which renders the MEMS capable of three-dimensional movement. Studies that focus on the mechanical interactions between two materials at an atomic scale often use scanning probe microscopy (SPM), scanning tunneling microscopy (STM), and atomic force microscopy (AFM) due to their higher precision during tests. The actuators and detection methods in these instruments are useful references for the development of in-situ TEM holders.

For actuation, in 1997, Kizuka et al. [42] exploited piezo tubes to achieve three-directional movement. The movable side was connected with a tube-type piezoelectric device and a microscrew motor for the fine and coarse displacement control, respectively. In 2003, a TEM holder was developed by an extremely compact STM design, which achieved both coarse and fine alignment by a single piezo tube [59]. The setup was also developed with a vision feedback system to achieve an automated closed-loop nanopositioning [60]. Besides piezoelectric actuators, Lobato-Dauzier et al. [61] attempted to introduce a novel actuation principle that exploits the internal magnetic field in TEM. The moving beam would bend due to a Laplace force when currents flowed. Furthermore, the force direction could be altered by current direction. The magnetic field can also be utilized to realize the lateral force-actuated function for quantitative friction tests [46]. When a current flowed through the silver asperity and tungsten flat punch under a magnetic field, the sliding was actuated by a Lorentz force, and the friction force could be determined by tracking the elastic deflection of the cantilever on the side of silver asperity from an in-situ TEM video. However, magnetic actuators have limited displacement, and can only apply force in uniaxial directions. Until now, the piezoelectric actuator is still irreplaceable in achieving high precision, stability, and flexibility when positioning the probe in in-situ TEM holders.

For force detection, in 1998, Wall and Dahmen [62] designed a TEM holder and achieved the function of nanoindentation in a high voltage TEM. Later, the TEM holder was developed for lower voltage, and a quantitative force sensor was added for in-situ nanoindentation studies [63]. The actuator was calibrated by in-situ bending microscale silicon cantilevers. The quantitative force could be calculated by displacement of the probe and voltage of the piezoceramic actuator. In addition, another quantitative force acquirement method with a four-bar flexible hinge spring element [64] was widely used in TEM holders such as the nano-tribometer designed by Desai and Haque [65]. With this method, the lateral and normal forces cause the floating beam to displace in two directions, respectively. The displacements were obtained from the changes of capacitances, which were used to calculate the forces by multiplying the spring constants. Multiaxial force detection can be realized by using this method.

With recent advancements in in-situ TEM holders, there has been a gradual improvement in the precision of positioning and alignment, as well as the accuracy of force sensors. For example, the in-situ TEM holder of Hysitron PI95 PicoIndenter (Bruker, Billerica, MA, USA) adopts a piezo for fine positioning and is equipped with a force/displacement transducer. The MEMS transducer adopts a comb-drive electrostatic actuator and obtains electrostatic force from capacitance change, which shows a load resolution of 3 nN and displacement resolution of 0.02 nm. Exploiting this equipment, Fan et al. [33] obtained load-displacement curves while testing silicon pillars with and without carbon films and reported a nanoresponse of re-indentation caused by an adhesion behavior.

However, for nanocontacts or atomic contacts, the force is usually too small to be detected by MEMS-based sensors due to their limited resolution. To address this issue, the cantilever of AFM, which has a very small stiffness, can be used in combination with a series of TEM images to detect nano-Newton force [66–68]. Wang and Mao [48,69] acquired nanoscale lateral force by combining in-situ TEM and AFM measurements, which provided direct real-time observations of atomic-scale interfacial structures during sliding processes. Atomistic simulation revealed that the nanoscale tip exhibited a zigzag behavior through two slipping steps to complete one full-period friction [69]. The accumulation and release of strain energy on the friction interface underwent an asynchronous evolution, accompanied by an inhomogeneous stress distribution and a non-uniform movement of interface atoms. The formation of a loosely packed interfacial layer between two metallic asperities that enabled a low friction under tensile stress was demonstrated [48]. This showed the prospect of studies on atomic contact mechanisms, which can assist to break the size barrier of nanodevices.

In summary, the main advantage of sample-integrated MEMS devices is to avoid issues of positioning and alignment, which are widely used in tensile tests to simplify the process of in-situ TEM experiments. The integral designs also provide the sample-integrated MEMS devices with exceptional stability but limit the flexibility in experiments. Additionally, the preparation process for sample-integrated MEMS devices is more complex compared to the sample-separated ones. Sample-separated MEMS devices can be used to conduct the in-situ TEM nanoindentation, nanofriction, and nanowear tests, which are essential in investigating the mechanism of nanocontacts and tribological behaviors. One of their drawbacks is the need for precise actuation and detection, which is demanding for MEMS, and the positioning and alignment during the experiment process is also time-consuming. With the development of various actuators and sensors, resolution has improved, which facilitates in-situ TEM nanomechanical and nanotribological studies. It is only with nano- and atomic-scale in-situ studies that interfacial properties can be clarified from the perspective of interface nanostructure effects, which is crucial for the development of surface engineering.

Furthermore, carbon-based contact interfaces are heavily influenced by different physical fields, such as electric [70], thermal [71], and optical [72] ones. In-situ TEM electromechanical contact tests were first conducted by Alsem et al. [73]. A movable probe was exploited to establish the site-specific electrical contact, and the Pt/Pt interfaces were examined [74]. Their results showed that the electron transport in device-relevant platinum nanocontacts can be significantly limited by the presence and persistence of surface species, resulting in a tunneling theory that better describes current flows than a ballistic electron transport, even for cleaned pure-platinum surfaces. In addition, thermal [75] and optical [76] MEMS devices have also been developed in in-situ TEM studies. In the future, multi-physical fields integrated with in-situ TEM mechanical and tribological tests is expected.

3. Mechanical Properties

The in-situ TEM method provides an opportunity to understand the outstanding mechanical properties of carbon-based materials, to establish the relationship between nanostructure and properties, and to reveal the difference and similarities between carbon-based materials at a micro-/nanoscale. In this section, the in-situ mechanical properties of carbon-based materials with different nanostructures are reviewed from the perspectives of strength and adhesion. Strength is a material property that describes the response to external forces. It is an inherent characteristic, such as elastic modulus, hardness, fracture strength, and yield strength. Adhesion is a non-inherent characteristic. It exists at the interface of two materials and is affected by the inherent properties of the materials such as their nanostructure and topography, as well as their contact conditions such as load, contact area, and counterpart material.

3.1. Strength

The strength of carbon-based materials is investigated with elastic and plastic deformation, which largely depend on the differences in nanostructure and can be easily confirmed by in-situ TEM observations. Simple nanostructures such as CNT and graphene have the highest strength. Using in-situ TEM compression tests, Jensen et al. [30] found that the buckling of multi-walled carbon nanotubes (MWNT) occurred at first, which is in accordance with classical elastic theory, as shown in Figure 3a. Then, a kinking appeared, along with permanent plastic deformation, as shown from the in-situ TEM observation. Through in-situ TEM nanoindentation tests, Tsai et al. [77] found that the type of deformation caused by kinking depends on the tube's thickness. The V-shaped kinks of thin-walled MWNTs were entirely reversible without residual plastic deformation following unloading [78]. However, with compressed thick-walled MWNTs, the buckling-induced complex Yoshimura patterns were observed in-situ at the compressive side rather than at the kinks. Zhao et al. [79] conducted in-situ TEM compression tests on thick-walled MWNTs and observed two fracture modes: planar fracture mode and shell-by-shell fracture mode. Planar fracture occurred due to the defects in MWNTs, while shell-by-shell fracture was caused by the outer layers of MWNTs suffering the most tension force. It should be noted that the effects of thickness on fracture properties also exist in multi-layered graphene. Li et al. [31] performed an in-situ TEM tensile test on a multi-layered graphene and claimed that the fracture strengths of graphene nanosheets decrease as the thickness increases due to the defects and fracture layers with a power law trend. The thick-layered graphene fractured with its brittle characteristic, and the thin-layered graphene showed obvious delamination between the atomic layers at the fracture site. Jang et al. [80] also discovered an asynchronous crack propagated along independent paths, which happened in a multi-layered graphene and caused interlayer slippages and dissipated a part of its energy. Additionally, Wei et al. [81] executed in-situ TEM tensile tests on a notched multi-layered graphene and observed the nanostructure of its fracture and crack edges. It was suggested that the higher fracture toughness was attributed to the disordered layers. By combining in-situ videos with finite element methods, the fracture toughness of the multi-layered graphene was determined to be 12.0 ± 3.9 MPa$\sqrt{m}$.

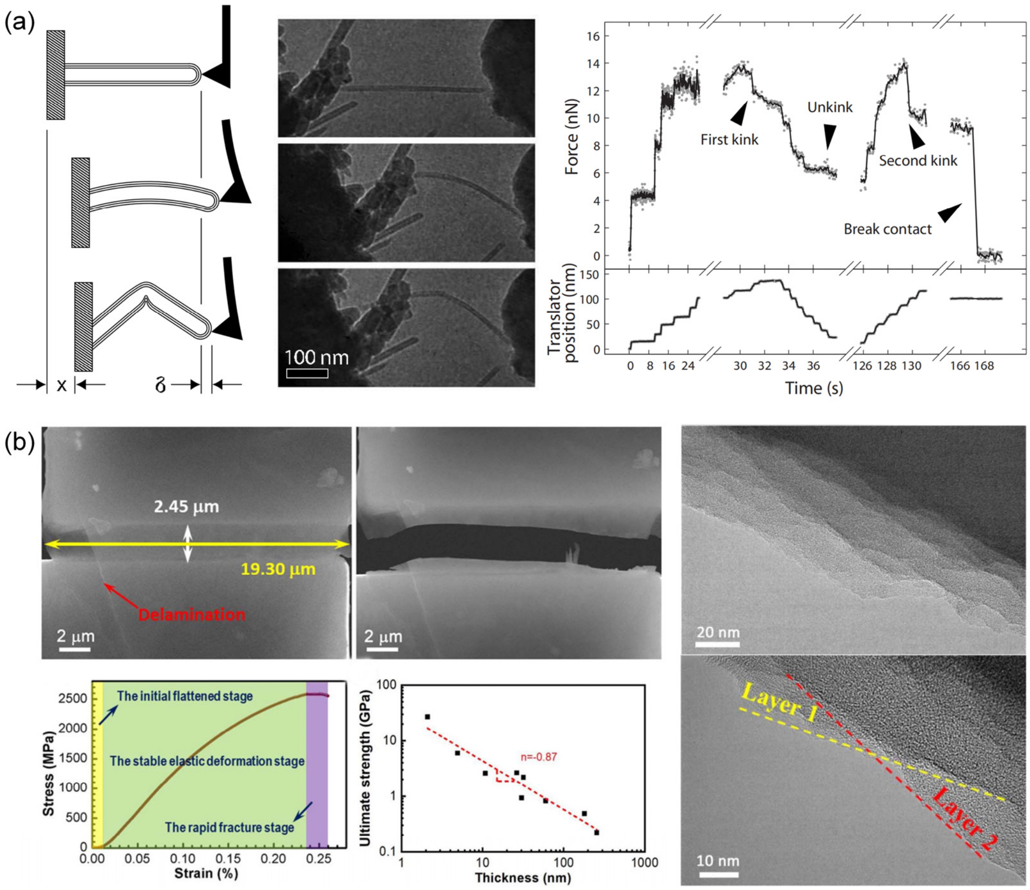

Figure 3. The in-situ TEM studies of (**a**) MWNTs [30] and (**b**) a multi-layered graphene [31]. (**a**) A buckling and kinking of MWNTs along with the corresponding curves of force and position with time. x: Distance of actuator, δ: Distance of AFM cantilever. (**b**) TEM images before and after tensile tests, the curves of stress–strain and strength–thickness, and high-resolution TEM images of a fracture edge. Reproduced with permission from Ref. [30]. American Physical Society, 2007; and Ref. [31]. IOP Publishing, 2019.

Furthermore, by exploiting the in-situ TEM tensile tests, the fracture strength of single-walled carbon nanotubes (SWNT) with visibly perfect shell structures measured directly were from 25 GPa to 100 GPa [82]. The fracture strength values were calculated by dividing the failure load by the cross-sectional area S of a single shell, $S = pdt$, where d is a diameter of the tube that was obtained directly from the in-situ TEM video, and t is a shell thickness (by taking the inter-layer separation of graphite, 0.34 nm). In addition, the mean single-shell failure of the MWNT was ~100 GPa, which agreed with the quantum-mechanical estimation of small-defects-contained strength [1]. The Young's modulus of a monolayer graphene was obtained from the in-situ SEM tensile test, which was close to the theoretical value of 1 TPa [2]. These data indicate that the long-standing gap between theory and experiment can be broken with the help of in-situ experiments, especially with the high-resolution of in-situ TEM. Furthermore, they directly evidence the need to study the effects of nanostructures on the mechanical properties of carbon-based materials.

Since carbon atom has three different kinds of hybridization that connect with each other in different types, structural variation strongly affects their properties. By carrying out in-situ TEM tensile tests on CNTs with different nanostructures, the fracture strength of nanotubes was confirmed to improve ten times more by inducing the formation of cross-linking structures between the shells [83] and can also be tailored by tuning a precise diameter through irradiation/annealing methods [84]. The chemical group, on the other hand, changes the carbon nanostructure. The functional group of multi-layered graphene oxides (GO) revealed a crack-arresting effect, which resulted in a nonlinear stress–strain response during an in-situ TEM tensile test [85–87].

More complex carbon nanostructures such as *a*-*C* can often be altered by stress, thermal, or other physical fields in order to dissipate energy. This allows for more distinctive and flexible adjustments to the strength of materials with different nanostructures. Wang et al. [32] proved the formation of graphitic nanocrystallites in the *a*-*C* pillar under a pure compression force field. The high-resolution TEM observation shown in Figure 4a reveals the dispersed nanocrystallites in the *a*-*C* matrix at the deformed regions. In addition, the formed graphite (001) lattice was oriented along the direction of a maximum resolved shear stress, which was consistent with the graphitization of the *a*-*C* film exhibited at a macroscale [88]. Moreover, Wan et al. [89] found that electron irradiation can promote the transformation of *a*-*C* to ordered small-sized graphene flakes. In Figure 4b, under a uniaxial strain, these graphene flakes connected and produced a high-oriented structure. This ordered graphene nanostructure within the carbon-based materials can enhance the strength, just as Beese et al. [90] found that the strength and stiffness of carbon nanofibers depend on the degree of orientation of the (002) graphitic planes along the tensile axis.

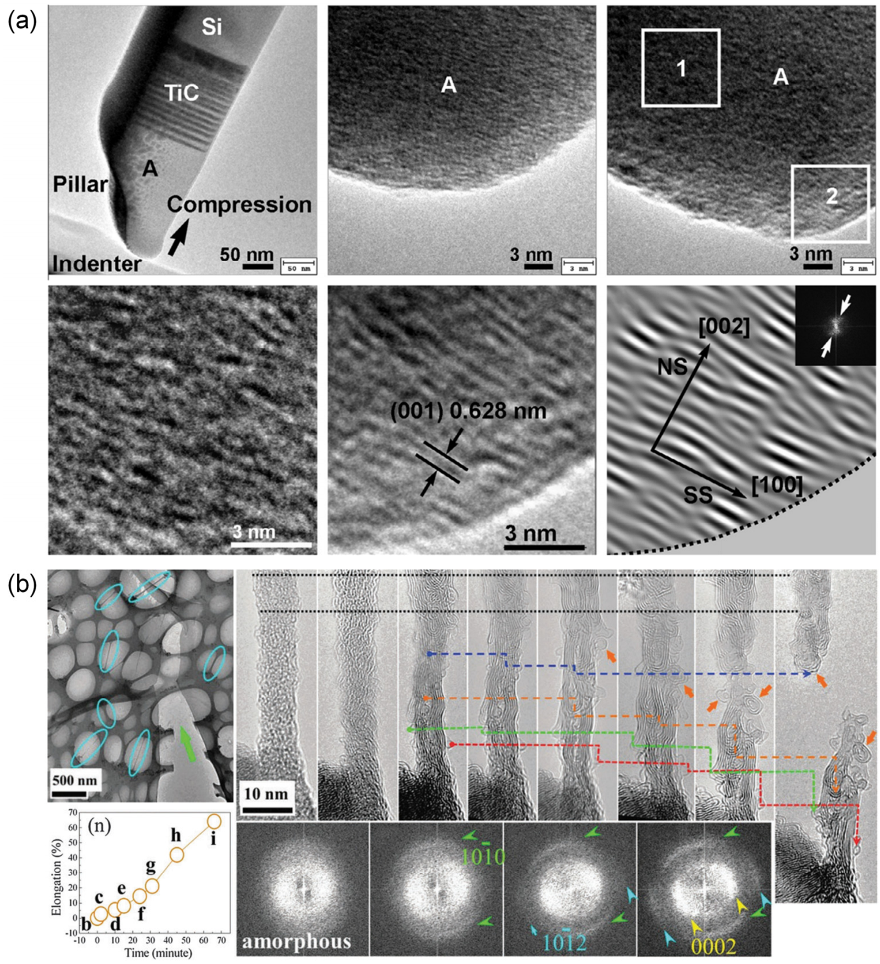

Figure 4. The strain-induced oriented graphene lattice of *a*-*C* material under (**a**) compression [32] and (**b**) tension [89] by in-situ TEM studies. (**a**) High-resolution TEM images at the contact position. A: *a*-*C*, 1,2: Areas for high-resolution TEM observation. (**b**) High-resolution TEM images of the fracture process. "b–i": The corresponding elongation with a series of high-resolution TEM images. Four colored lines were used to depict the movement of four positions during the tensile process. Reproduced with permission from Ref. [32]. Elsevier, 2014; and Ref. [89]. Royal Society of Chemistry, 2016.

In-situ TEM tensile and compression tests provide a means to obtain the strength of carbon-based materials, to analyze the evolution of nanostructures, and to clarify failure mechanisms. They play a crucial role in understanding the inherent characteristics of carbon-based materials.

3.2. Adhesion

Adhesion between two surfaces is an important property in contact mechanics, which has a significant impact on the tribological behavior of materials. In addition, adhesion is usually described by two parameters: the strength and length scale of the interaction, which are expressed as the intrinsic work and the range of adhesion, respectively. In-situ TEM methods allow for a better understanding of adhesion at the nanoscale, which is also essential for comprehending the adhesive properties of bulk materials at a larger scale.

The first parameter is the work of adhesion, whose accurate description is needed to determine the effect of atomic-scale roughness—a significant factor at the nanoscale. Jacobs et al. [34] conducted in-situ nanoindentation tests to investigate the effect of nanometer- and subnanometer-scale roughness on the adhesion of single asperity, by examining the contact between silicon tips and diamond-like carbon (DLC) films or ultrananocrystalline diamond (UNCD) films. The roughness was quantified from high-resolution TEM images, and the work of adhesion was calculated. The results showed that the work of adhesion decreased with the increase of roughness. Subsequently, to more accurately describe the adhesion phenomenon at a nanometer-scale, the pull-off forces and snap-in distances were measured from an in-situ TEM video and were used to calculate the intrinsic work of adhesion and the range of adhesion [91]. Furthermore, the snap-in/pull-off numerical adhesion parameter (SNAP) was exploited to study the interface between the silicon and diamond. The calculated work values of adhesion were 70% higher than when using a conventional paraboloidal asperity model [92]. These studies prove the important role of in-situ TEM methods in measuring the work of adhesion.

Another important parameter to study interfacial adhesion is the range of adhesion, which is related to the chemical bonding at the contact interface. Bernal and Carpick et al. [35,93] studied the influence of chemical bonding on the variability of DLC nanoscale adhesion by in-situ TEM nanoindentation tests. The reason for this was due to the roughness and the stochastic nature of atomic bonding. The roughness directly affected the number of interfacial atoms, while the stochastic nature meant the formation of a bond between unsaturated carbon atoms across the interface. The interfacial bonding could be determined by the local energy landscape of the atom affected by the nearest neighbors and their termination, and also how the energy landscape was changed by interactions and stresses with the tip's contact. The atomic bonding played a role in adhesion, especially for non-passivated surfaces [94]. In addition, the sliding increased the interfacial covalent-bond formation due to the effect of shear stress, which lowered the barrier of forming covalent bonds across the interface. Therefore, the adhesion increased with the sliding speed and normal stress due to the increasing of the number of bonds. Vishnubhotla et al. [95] further verified that a large compressive stress applied before separation would lead to covalent bonds across the silicon/diamond interface. The stress-dependence of covalent bonds was consistent with the trend areal density of in-contact atoms measured in an MD simulation. The phenomenon of sliding increasing the number of covalent bonds also existed in silicon/silicon nanocontacts, which caused the adhesion to increase by about 19 times on average compared to non-sliding [96]. Liang et al. [97] also confirmed the adhesion mechanism at the *a-C*/diamond interface. During their in-situ TEM experiments, the initially low adhesion of the *a-C*/diamond interface rapidly increased with additional shear stress caused by high stresses. The reason for this was ascribed to the covalent bonds formed with the exposed sp^3-rich layer, since a sp^2-rich layer with lower surface energy was worn out with the high contact stress. From the work of adhesion and the range of adhesion, adhesion properties can be quantitatively explained. The nanoresponse of re-indentation phenomena at the microscale can be declared with the work of adhesion [33]. Figure 5a exhibits a series of TEM images during an in-situ nanoindentation process. At the unloading period in Figure 5b, the pull-off force caused a sudden drop in displacement and an external loading-force change from tension to compression, which led to the probe's re-indentation into the surface. Furthermore, the work of adhesion can be calculated quantitatively from the re-indentation loop in load–displacement curves, shown in Figure 5c. It was found that the silicon pillars with carbon films exhibited a lower adhesive force and reduced the impact of re-indentation to the silicon substrate.

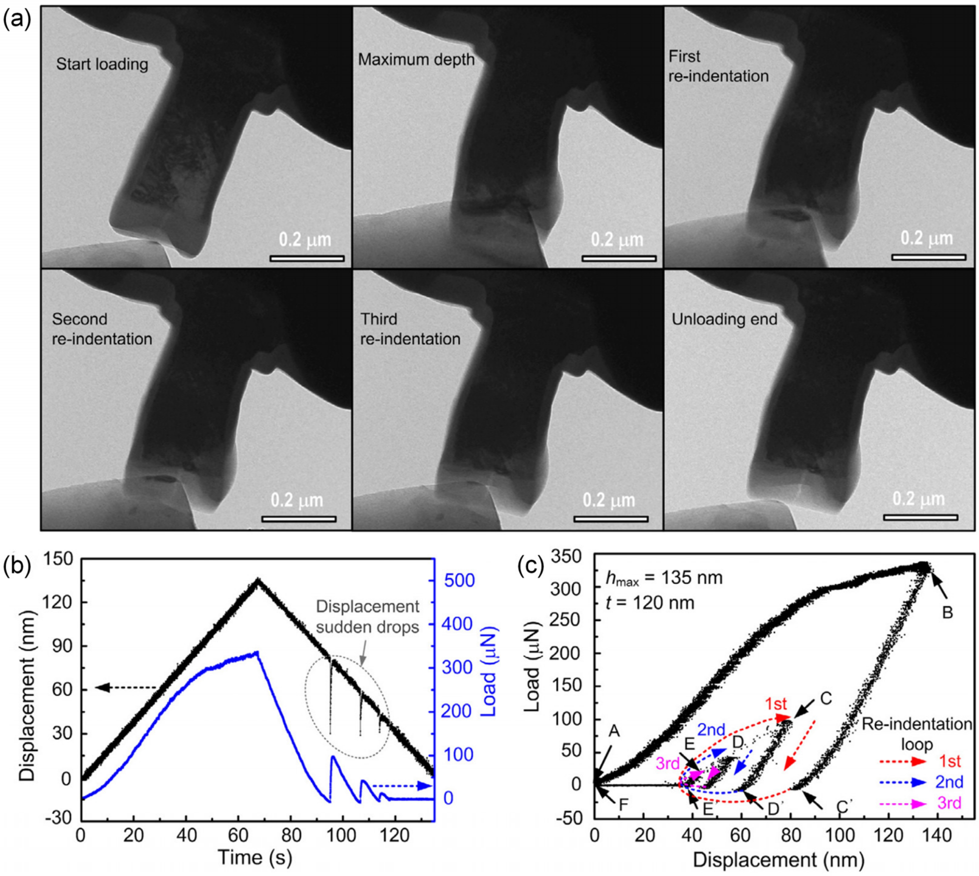

Figure 5. (**a**) Series of TEM images during the in-situ nanoindentation process. (**b**) Curves of displacement and load with time. (**c**) Load–displacement curve. "A–F": The order of nanoindentation process. "C′–E′": Adhesive positions. The Reproduced with permission from Ref. [33]. Elsevier, 2016.

By in-situ TEM nanoindentation tests, the adhesions of carbon-based materials can be analyzed by the work of adhesion and the range of adhesion, which have a significant effect on promoting the application of carbon-based materials at the micro-/nanoscale. Furthermore, they can also be developed to investigate the adhesion properties of more materials with different nanostructures.

To sum up, the mechanical properties can be divided into the inherent characteristic of strength and non-inherent characteristic of adhesion. Strength is mainly decided by the interior nanostructure, while adhesion is affected by surface nanostructures, topography, load, and contact area. For the measurement of inherent characteristics, the strength of carbon-based materials can be better understood with in-situ observations on deformation behaviors, especially at the micro-/nanoscale, such as the kinking behaviors of CNTs with different wall thicknesses, and the differences of fracture strength caused by defects of various extents. In addition, by exploiting in-situ TEM tensile tests, a measured fracture strength of SWNT conforms to the theoretical value, which breaks the long-standing gap between theory and experiments. Moreover, in-situ observations also directly evidence the stress-induced transformation of nanostructures. For the measurement of adhesion, one of the advantages is its assistance from in-situ observations. The effect of nano-/atomic roughness and re-indentation phenomena are both clarified. It is noteworthy that the dispersion of adhesions is strongly related to the number of covalent bonds across the interfaces, which is mainly affected by nanostructures.

As of now, the main challenge is to establish a comprehensive understanding of carbon nanostructures. By conducting in-situ TEM tensile, compression, and nanoindentation tests, the mechanical behaviors of nanostructures such as CNT, graphene, and amorphous have been obtained and analyzed. However, it is important to note that mechanical behaviors can also be affected by the variations of nanostructures. Firstly, the imperfection of carbon nanostructures itself leads to variations. For example, defects in CNTs can reduce fracture strength, while the cross-linking structure across the shells can increase the fracture strength. Secondly, the second element can also cause variations. For instance, the functional group of GO has a crack-arresting effect. Lastly, carbon-based materials composed of different nanostructures, and thus, UNCD and DLC films, exhibit different adhesion behaviors. Overall, there are still many unclear aspects of carbon nanostructures that can affect the mechanical properties of carbon-based materials. Exploiting in-situ TEM methods can effectively modify carbon nanostructures. This plays a crucial role in promoting the application of carbon-based materials.

4. Tribological Behaviors

In-situ TEM nanofriction and nanowear tests provide a direct method for understanding contact interfaces during the sliding process. They allow one to visualize and perceive the underlying physical processes of carbon-based materials and help to conclude the mechanism at the multiscale. In this section, the tribological behaviors of carbon-based materials are classified into two categories: friction and wear.

4.1. Friction

Friction is an essential factor in illuminating the tribological mechanism. By acquiring the friction force, calculating the shear stress, and analyzing the corresponding wear state from in-situ TEM observations, the sliding process can be carefully examined. At the micro-/nanoscale, the fluctuations of the sliding process are magnified and exhibit distinct stick and slip stages. Therefore, in-situ TEM tribological studies mainly focus on the superlubricity and the stick–slip friction of carbon-based materials.

For the superlubricity, Liu et al. [98] demonstrated the superlubricity of highly ordered pyrolytic graphite (HOPG) in an incommensurate direction by an in-situ SEM test, with a sixfold symmetry of the self-retraction between graphite layers. Weaker van der Waals bonds exist between adjacent graphene layers and also exist between graphene- and carbon-contaminating molecules. The results were exploited to realize the mechanically cleaned graphene layer surface by an in-situ piezo-driven nanopositioning system [37]. Furthermore, the van der Waals bonds were also the main bonds across the shells of CNTs. For MWNT, Kis et al. [99] examined the friction between shells by conducting the cyclic telescoping motions of the MWNT. The upper limit value was 1.4×10^{-15} N/atom, which exhibited a super-low friction between the core and the outer shells and can be adjusted by stable defects. The defects were formed by generating dangling bonds first and then self-repaired to optimize the atomic structure and restored smooth motion. For DWNT, Lin et al. [36] also performed torsional motions of DWNT shells by a torque applying on the outer shell to infer the shear modulus between shells, the van der Waals interactions, and the reliable models of the lattice strain. The average kinetic friction force was $(2.6 \pm 1.0) \times 10^{-15}$ N/atom, which may be due to the randomness of the sample and the stability of the interaction area during the tests.

For stick–slip friction, Fan et al. [100] illuminated the origin of stick–slip friction of sp^2 nanocrystallited carbon films. By performing in-situ TEM nanofriction tests on two different sp^2 nanocrystallited carbon films, shear stresses were calculated, as shown in Figure 6a,b. At the stick stage, the shear stress gradually increased as the contact strengthened until the shear strength broke the interfacial adhesion. At the slip stage, the shear stress decreased and was accompanied by film deformation. The film deformations were obtained from an in-situ video and are shown in Figure 6c,d. The adhesive deformation resulted in a large stick–slip step while ploughing deformation led to a smoother step, and the deformation type was due to film density, and surface roughness and hardness, which was affected by the size of sp^2 nanocrystallites.

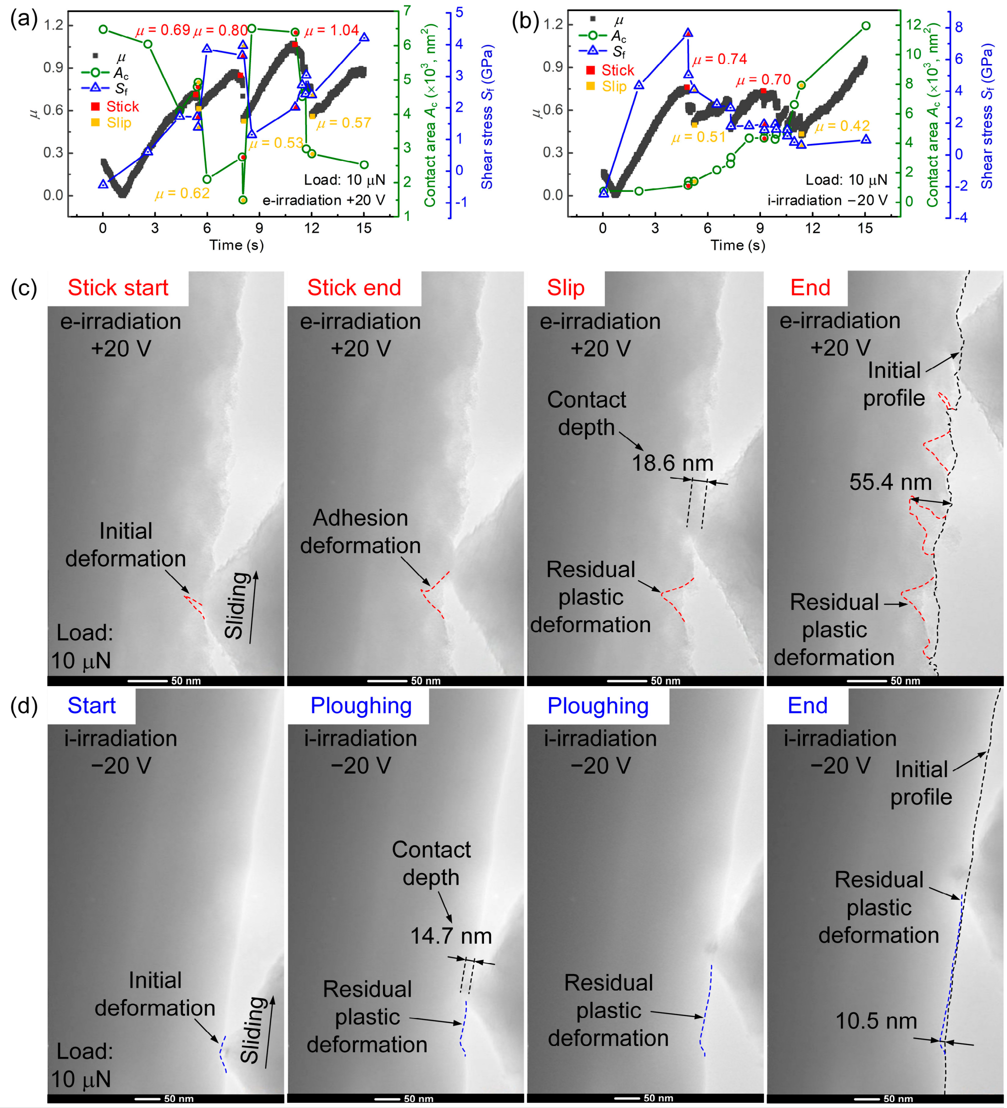

Figure 6. (**a**,**b**) Friction coefficient of two different carbon films with the corresponding variations of contact area and shear stress under the load of 10 μN. (**c**) Large area adhesion of plastic deformations caused by stick–slip. (**d**) Ploughing of plastic deformations with a stable sliding process. Reproduced with permission from Ref. [96]. Springer Nature, 2022.

Furthermore, Hu et al. [38] confirmed that the larger size of sp^2 nanocrystallites can facilitate the formation of transfer films for a stable low friction with in-situ TEM nanofriction tests. The in-situ TEM observations showed that the sp^2 nanocrystallites lay down, paralleled to the sliding direction, and sheared under the compressive and shear stresses. The formation of transfer films can decrease the friction coefficient. Figure 7 exhibits high-resolution TEM images when the scratching on sp^2 nanocrystallited film finished and the sp^2 nanocrystallites were observed to be parallel to the interface. However, for the other different nanostructures, monocrystalline silicon is hard to form lamella structures, and the *a*-C film needs high stress and a longer sliding distance to form transfer films.

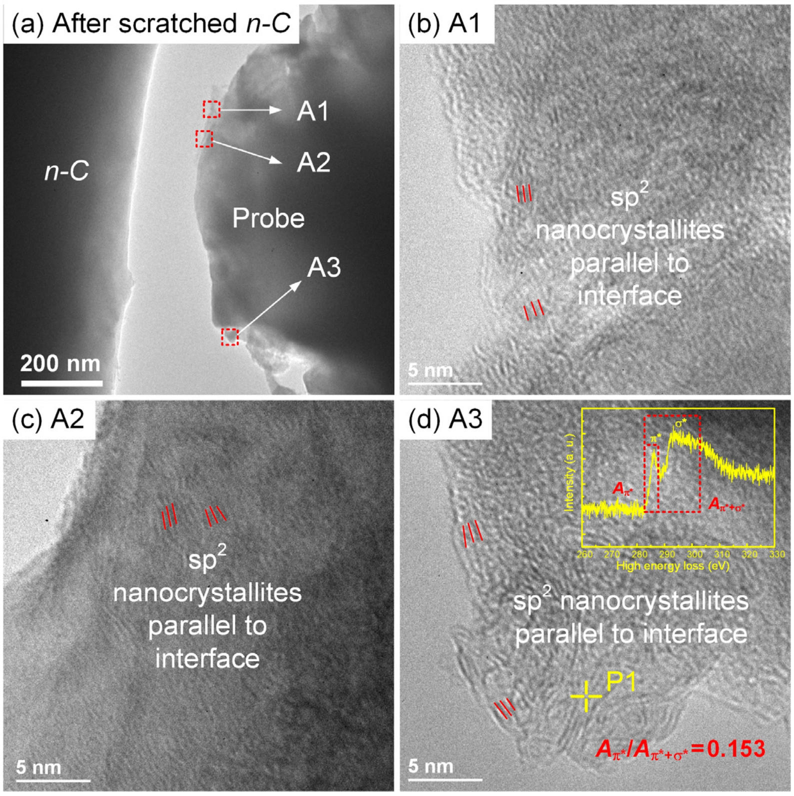

Figure 7. (**a**) TEM images of when the scratching on the sp^2 nanocrystallited film finished. (**b**–**d**) High-resolution TEM images of the different areas with transfer films labeled in (**a**), respectively. Reproduced with permission from Ref. [38]. Elsevier, 2022.

For the widely used DLC structure, the interface normally shows stick–slip friction. Sato et al. [101] found that the friction forces of DLC films against DLC films exhibited a large stick–slip phenomenon. Through an in-situ TEM observation of the contact interface, it was found that wear particles of 20–50 nm appeared after a sliding distance of 500 nm. Then, the particles rolled, rotated, and slipped when the two surfaces contacted and slid, which caused the friction force to exhibit a serious stick–slip phenomenon. At the nanoscale, although the applying load was just several tens of nano newtons, it was enough to cause very high stresses and permanent deformation. In addition, Hintsala et al. [102] used a wedge diamond indenter in-situ that scratched a perpendicular magnetic recording film in TEM, and the stick–slip mechanism was induced by a critical ratio of lateral to normal force. At low load forces, the DLC coating and asperities in the recording layer were removed. With the increase of load and displacement, the work of stick–slip deformation increased. Meanwhile, at higher load forces, the critical friction force induced a stick–slip motion that suddenly increased, which corresponds to the phenomenon of grain reorientation and debonding of the recording layer.

At the micro-/nanoscale, the tribological performance of carbon-based materials and superlubricity is usually exhibited within a carbon crystal structure such as a multi-layered graphene and CNTs. Meanwhile, the stick–slip friction occurs at different degrees when scratched for the amorphous and sp^2 nanocrystallites embedded in an amorphous structure. By employing in-situ TEM tribological experiments, the contact and shear deformation mechanisms of carbon-based material can gather powerful evidence to declare the phenomenon at the macroscale, which can also contribute to a wider utilization of carbon-based material for energy conservation.

4.2. Wear

The material removal process is influenced by various contact conditions, including the applied load, sliding speed, surface morphology, temperature, environment, and more.

However, the removal pattern is primarily determined by the nanostructure of carbon-based materials, either through single-atom processes or the collective motion of atoms. The basic nanostructures of carbon are amorphous, graphite, and diamond, each of which demonstrate different removal mechanisms during the sliding process.

For the wear of *a*-*C*, Wang et al. [39] conducted in-situ nanofriction tests on ultrathin *a*-*C* films by cyclic nanoscale loading. The wear debris from a single fracture was generally amorphous in structure, and the degree of graphitic ordering in wear debris increased with prolonging cyclic lateral loading. As shown in Figure 8a, the wear debris transferred to its counterpart, forming onion-like carbon (OLC) structures. Moreover, an atom-by-atom wear of *a*-*C* was present. Liu et al. [103] performed in-situ nanowear tests and showed the strong effect of contact stress on wear. This supported the mechanism involving high contact stress increasing covalent bonds at the *a*-*C*/diamond interface and causing higher adhesion.

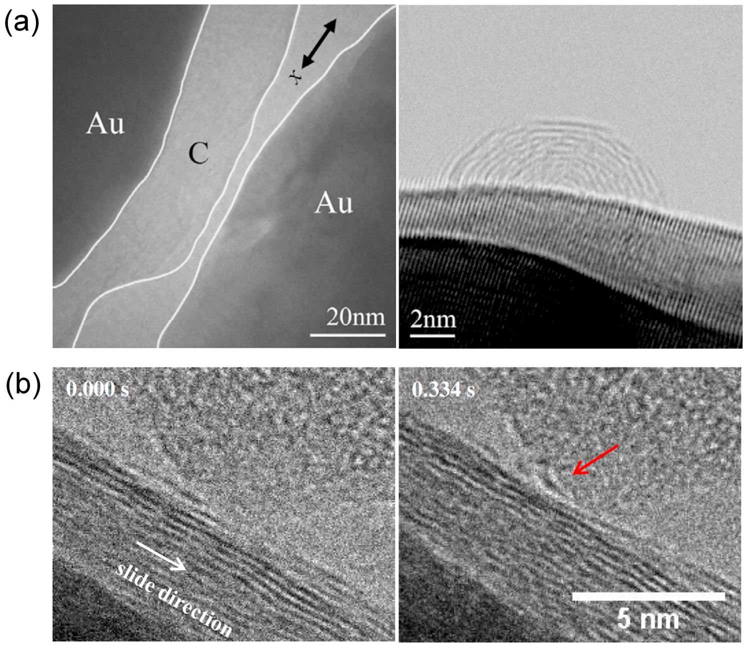

Figure 8. Wear properties of (**a**) *a*-*C* films [39] and (**b**) HOPG [40]. (**a**) High-resolution TEM images of graphitic ordering to form a carbon onion under cyclic lateral loading. x: Sliding direction. (**b**) High-resolution TEM images of monolayer transferring during the sliding process. Red arrow: Transferred monolayer. Reproduced with permission from Ref. [39]. IOP Publishing, 2009; and Ref. [40]. Springer Nature, 2015.

Considering the passivation of chemical groups, in-situ TEM nanowear tests were performed on DLC films deposited using the plasma-enhanced chemical vapor deposition (PECVD) technique [104]. After high-resolution TEM observation and electron energy loss spectra (EELS) characterization, the tribolayers were confirmed at the sliding interface of the tungsten tip due to local mechanical excitation, which is consistent with graphitization effects [88]. Additionally, the film with high hydrogen content exhibited significantly less wear debris on the tungsten tip. M'ndange-Pfupfu et al. [105] conducted in-situ TEM nanowear tests on deposited DLC films using the magnetron sputtering technique, which revealed that the rate of phase transformation from sp^3 to sp^2 bonding was quantified as a volume of 0.009–0.018% transformed per sliding pass and exhibited a linear trend of transformation rate. Because the hydrogen-free "dead zone on the top surface" [106] was smaller, constant hydrogen migration was exhibited at the surface. Meanwhile, for DLC films prepared by PECVD [104], the phase transformation was slow at first but rapidly increased after a certain time as the dead zone was much thicker. The wear behaviors of DLC films in wet hydrogen and wet nitrogen were also observed in-situ by exploiting an environmental transmission electron microscope (ETEM) [107]. By observing the sliding fracture zones, the difference of wear behaviors directly indicated that the wear was retarded in wet hydrogen and accelerated in wet nitrogen, which was in accordance with the expectation of many length scales [108]. With the assistance of in-situ TEM studies, the mechanisms at the contact interface can easily be clarified.

For the wear of graphite, Merkle et al. [109] used a single tungsten asperity in-situ slide on HOPG in TEM. Wear of the HOPG was observed by graphitic flakes transferred to the tungsten tip, and the removal of sheets was ten basal layers in thickness due to the interfacial dislocation standoff distances. Afterwards, the transferring of graphene was also observed through a tip to the in-situ scratch of the multi-layer graphene, which is shown in Figure 8b [40]. At the beginning, the single top sheet attached to the tip and slid relatively to the second sheet. A crumple appeared in the scratch direction and increased gradually until the shear stress was high enough to fracture the top sheet at the crumple position, and then the transferring process finished. Comparing this with the same structure of lamella molybdenum disulfide, graphene was easier to crumple during the sliding process.

For the wear of diamond structures, Bernal et al. [41] in-situ observed the evolution of morphological and crystal structures during the sliding process in TEM and demonstrated that amorphization, gradual atomic-scale wear, and fractures appeared in the nanoscale wear process of UNCD asperities. Amorphous debris could be observed around the contact area and accumulated at the contact edges. In addition, an observation of embedded crystallites in the amorphous debris meant that fractures existed. Moreover, the wear rate of UNCD asperities were also quantified, which decreased with the sliding distance. For two UNCD asperities, the wear rate can decrease to 10^{-3}–10^{-2} mm^3/Nm. Meanwhile, for one UNCD asperity against a UNCD flat, the wear rate can decrease to ~10^{-4} mm^3/Nm.

It is shown from these studies that different carbon nanostructures usually exhibit different removal types, such as fractures, layer-by-layer removals, and atom-by-atom removals. All of the removal mechanisms were related to the defects, the ratio of sp^2/sp^3 bonds, the existence or inexistence of nanocrystallites, the stress-induced nanostructure evolution, and so on. By exploiting in-situ TEM nanowear tests, the effect of nanostructure in the material-removal process is elucidated and helps to develop the anti-wear properties of materials at the micro-/nanoscale.

The contact interfaces are extraordinarily important in studying the tribological behaviors of carbon-based materials. However, most tribological studies rely on ex-situ experiments, even at the nanoscale, which may have several problems. The first problem is the confirmation of contact depth and contact area. In-situ TEM observations of the nanofriction process allows for the extraction of contact depth from in-situ TEM videos and the contact area can be calculated by fitting the shape of the probe, which is more accurate than theoretical models such as the Hertzian, Johnson–Kendall–Roberts (JKR) and Derjaguin–Muller–Toporov (DMT) models. The second problem is the characterization of wear volume and nanostructures. Material-removal processes of carbon-based materials are usually classified as fractures, layer-by-layer, and atom-by-atom removals. In addition, the potential variation of nanostructures in contact surfaces also needs to be examined. These characterizations can be performed directly in TEM by taking advantage of high-resolution observations and the EELS spectrum. The last problem is the effect of other elements. A high-vacuum environment can create a clear contact interface without contamination from other elements, especially in easily affected carbon-based interfaces, which can help to clarify the mechanism of the carbon nanostructure itself. To summarize, the powerful functions of in-situ TEM methods still have the potential to elucidate carbon-based interfaces with different nanostructures. This contributes to the development of self-lubrication materials and expands the mechanical and tribological application range of carbon-based materials.

5. Conclusions and Outlooks

5.1. Conclusions

This work provided an overview of in-situ TEM studies on the mechanical and tribological behaviors of carbon-based materials, which are divided into three sections: quantitative actuation and detection, mechanical properties, and tribological behaviors. The summaries are as follows:

(1) MEMS devices used in in-situ TEM experiments consist of sample-integrated MEMS and sample-separated MEMS. The sample-integrated ones have been widely used in tensile tests to avoid positioning and alignment problems, while the sample-separated ones are more flexible and can be used in nanoindentation, nanoscratch, and nanowear tests.
(2) The strength and adhesion of carbon-based materials exhibit strong relationships with the nanostructure. In-situ TEM tensile, compression, and nanoindentation tests were conducted to study the unusual strengths of simple nanostructures such as CNT and graphene, the reconstruction of complex nanostructures, the intrinsic works, and adhesion range of different carbon-based interfaces.
(3) The nanostructure also significantly affects the friction and wear of carbon-based materials. In-situ observations of contact interfaces were used to investigate the superlubricity between CNT shells, the origin of stick–slip friction of different carbon films, the wear types of atom-by-atom removals, and the collective motion of atoms.

In-situ TEM studies have shed light on the strength, adhesion, friction, and wear of carbon-based materials with different nanostructures, which contributes to the scientific understanding of the underlying mechanism at the micro-/nanoscale.

5.2. Outlooks

This work focused primarily on the in-situ TEM mechanical and tribological studies of carbon-based materials and has limited contents about the studies on other materials or properties measured with different physical fields. In addition, to further advancing in-situ TEM research on carbon-based materials, the following lines of research are suggested:

(1) Conducting various in-situ TEM experiments to examine how defects and variations in nanostructures induced by factors such as electron and ion irradiation affect the mechanical and tribological behaviors of carbon-based materials. Furthermore, carbon-based materials composed of different nanostructures should also be included. This can lead to a clearer understanding of carbon-based materials.
(2) Using in-situ TEM to elucidate the contact and deformation mechanism of carbon-based contact interfaces with modified nanostructures is encouraged, as this can benefit the development of self-lubricated materials.
(3) Developing in-situ MEMS devices for multi-physical field experiments to conduct the in-situ TEM mechanical and tribological tests should also be prioritized. This is because carbon-based materials with different nanostructures exhibit different properties under different physical fields, and there is a lack of systematic experimental research on the nanocontact interface at multi-physical fields.

Therefore, based on the current in-situ TEM studies on the mechanical and tribological behaviors of carbon-based materials, there is still a lot of unexplored potential for in-situ TEM methods, particularly in understanding the carbon-based nanotribological interfaces at different physical fields, which plays the indispensable role in promoting the development and application of carbon-based materials in micro-/nano-devices and holds significant importance for nanosurface science and engineering.

Author Contributions: Writing—original draft preparation, Z.H.; writing—review and editing, X.F.; supervision, D.D.; funding acquisition, X.F. All authors have read and agreed to the published version of the manuscript.

Funding: This work was financial supported by the National Natural Science Foundation of China (No. 51975382).

Data Availability Statement: Not applicable.

Acknowledgments: The authors wish to acknowledge the assistance on HRTEM-related content received from the Electron Microscope Center of the Shenzhen University.

Conflicts of Interest: The authors declare no conflict of interest.

References

1. Shirasu, K.; Kitayama, S.; Liu, F.; Yamamoto, G.; Hashida, T. Molecular dynamics simulations and theoretical model for engineering tensile properties of single-and multi-walled carbon nanotubes. *Nanomaterials* **2021**, *11*, 795. [CrossRef] [PubMed]
2. Cao, K.; Feng, S.Z.; Han, Y.; Gao, L.B.; Ly, T.H.; Xu, Z.P.; Lu, Y. Elastic straining of free-standing monolayer graphene. *Nat. Commun.* **2020**, *11*, 284. [CrossRef] [PubMed]
3. Zhan, H.; Chen, Y.W.; Shi, Q.Q.; Zhang, Y.; Mo, R.W.; Wang, J.N. Highly aligned and densified carbon nanotube films with superior thermal conductivity and mechanical strength. *Carbon* **2022**, *186*, 205–214. [CrossRef]
4. Diao, D.F.; Wang, C.; Fan, X. Frictional behavior of nanostructured carbon films. *Friction* **2013**, *1*, 63–71. [CrossRef]
5. Chen, C.; Xue, P.D.; Fan, X.; Wang, C.; Diao, D.F. Friction-induced rapid restructuring of graphene nanocrystallite cap layer at sliding surfaces: Short run-in period. *Carbon* **2018**, *130*, 215–221. [CrossRef]
6. Hu, Z.L.; Fan, X.; Chen, C. Multiscale frictional behaviors of sp^2 nanocrystallited carbon films with different ion irradiation densities. *Friction* **2021**, *9*, 1025–1037. [CrossRef]
7. Huang, Z.Q.; Xue, P.D.; Chen, C.; Diao, D.F. Rapid fabrication of ultra-wear-resistant graphene nanocrystallite film by direct laser writing. *Appl. Surf. Sci.* **2022**, *604*, 154658. [CrossRef]
8. Liu, M.; Su, W.L.; Qin, X.Z.; Cheng, K.; Ding, W.; Ma, L.; Cui, Z.; Chen, J.B.; Rao, J.J.; Ouyang, H.K.; et al. Mechanical/electrical characterization of ZnO nanomaterial based on AFM/nanomanipulator embedded in SEM. *Micromachines* **2021**, *12*, 248. [CrossRef]
9. Choi, M.G.; Park, S.; Lee, H.; Kim, S. Correlating surface structures and nanoscale friction of CVD multi-layered graphene. *Appl. Surf. Sci.* **2022**, *584*, 152572. [CrossRef]
10. Yang, X.; Zhu, W.L.; Zhu, Z.W.; Zhu, L.M. Design, assessment, and trajectory control of a novel decoupled robotic nanomanipulator. *IEEE-ASME Trans. Mechatron.* **2022**, *27*, 3999–4010. [CrossRef]
11. Yuan, S.; Wu, B.Y.; Wang, K.X.; Yu, P. Low-noise analysis and design for the sensing system of the nanomanipulation robot by AFM. In Proceedings of the 2022 IEEE International Conference on Robotics and Biomimetics (ROBIO), Jinghong, China, 5–9 December 2022; pp. 1491–1496.
12. Sampath, V.; von Gratowski, S.; Irzhak, A.; Lega, P.; Song, Z.; Cotta, M.A.; Koledov, V. Mechanical bottom-up nanoassembling and nanomanipulation using shape memory alloy nanogripper. In *Nanomaterials for Sensing and Optoelectronic Applications*; Elsevier: Amsterdam, The Netherlands, 2022; pp. 299–310.
13. Jacobs, T.D.B.; Martini, A. Measuring and understanding contact area at the nanoscale: A review. *Appl. Mech. Rev.* **2017**, *69*, 060802. [CrossRef]
14. Ellinas, K.; Gogolides, E. Ultra-low friction, superhydrophobic, plasma micro-nanotextured fluorinated ethylene propylene (FEP) surfaces. *Micro. Nano. Eng.* **2022**, *14*, 100104. [CrossRef]
15. Falk, K.; Reichenbach, T.; Gkagkas, K.; Moseler, M.; Moras, G. Relating dry friction to interdigitation of surface passivation species: A molecular dynamics study on amorphous carbon. *Materials* **2022**, *15*, 3247. [CrossRef]
16. Yin, S.C.; Wu, H.X.; Yi, X.B.; Huang, Z.Y.; Ye, C.P.; Li, P.F.; Zhang, Y.X.; Shi, J.Q.; Hua, K.; Wang, H.F. Enhanced graphene oxide adhesion on steel surface through boronizing functionalization treatment: Toward the robust ultralow friction. *Carbon* **2023**, *206*, 201–210. [CrossRef]
17. Zeng, X.Z.; Peng, Y.T.; Yu, M.C.; Lang, H.J.; Cao, X.A.; Zou, K. Dynamic sliding enhancement on the friction and adhesion of graphene, graphene oxide, and fluorinated graphene. *ACS Appl. Mater. Interfaces* **2018**, *10*, 8214–8224. [CrossRef]
18. Liu, S.W.; Wang, H.P.; Xu, Q.; Ma, T.B.; Yu, G.; Zhang, C.H.; Geng, D.C.; Yu, Z.W.; Zhang, S.G.; Wang, W.Z.; et al. Robust microscale superlubricity under high contact pressure enabled by graphene-coated microsphere. *Nat. Commun.* **2017**, *8*, 14029. [CrossRef]
19. Goryacheva, I.G.; Paggi, M.; Popov, V.L. Contact mechanics perspective of tribology. *Front. Mech. Eng.* **2021**, *7*, 649792. [CrossRef]
20. Dietzel, D.; Schwarz, U.D.; Schirmeisen, A. Nanotribological studies using nanoparticle manipulation: Principles and application to structural lubricity. *Friction* **2014**, *2*, 114–139. [CrossRef]
21. Li, S.Z.; Li, Q.Y.; Carpick, R.W.; Gumbsch, P.; Liu, X.Z.; Ding, X.D.; Sun, J.; Li, J. The evolving quality of frictional contact with graphene. *Nature* **2016**, *539*, 541–545. [CrossRef]
22. Liu, J.J.; Notbohm, J.K.; Carpick, R.W.; Turner, K.T. Method for characterizing nanoscale wear of atomic force microscope tips. *ACS Nano* **2010**, *4*, 3763–3772. [CrossRef]
23. Yang, Z.T.; Hu, Z.L.; Fan, X.; Chen, C. Parallel electricity at friction interface induced fast superlow friction of amorphous carbon films. *Appl. Surf. Sci.* **2022**, *577*, 151962. [CrossRef]
24. Chen, R.M.; Vishnubhotla, S.B.; Khanal, S.R.; Jacobs, T.D.B.; Martini, A. Quantifying the pressure-dependence of work of adhesion in silicon-diamond contacts. *Appl. Phys. Lett.* **2020**, *116*, 051602. [CrossRef]
25. Zhu, Y.T.; Yuan, D.D.; Zhang, H.; Xu, T.; Sun, L.T. Atomic-scale insights into the formation of 2D crystals from in situ transmission electron microscopy. *Nano Res.* **2021**, *14*, 1650–1658. [CrossRef]
26. Ngo, D.T.; Kuhn, L.T. In situ transmission electron microscopy for magnetic nanostructures. *Adv. Nat. Sci.-Nanosci. Nanotechnol.* **2016**, *7*, 045001. [CrossRef]
27. Tian, X.C.; Caruntu, G.; Kavey, B.; Tan, X.L. In situ TEM measurement of electrical properties of individual $BaTiO_3$ nanocubes. *Appl. Phys. Lett.* **2021**, *118*, 192901. [CrossRef]

28. Dong, H.; Xu, F.; Sun, Z.Q.; Wu, X.; Zhang, Q.B.; Zhai, Y.S.; Tan, X.D.; He, L.B.; Xu, T.; Zhang, Z.; et al. In situ interface engineering for probing the limit of quantum dot photovoltaic devices. *Nat. Nanotechnol.* **2019**, *14*, 950–956. [CrossRef]
29. Espinosa, I.P.M.; Azadehranjbar, S.; Ding, R.K.; Baker, A.J.; Jacobs, T.D.B.; Martini, A. Platinum nanoparticle compression: Combining in situ TEM and atomistic modeling. *Appl. Phys. Lett.* **2022**, *120*, 013101. [CrossRef]
30. Jensen, K.; Mickelson, W.; Kis, A.; Zettl, A. Buckling and kinking force measurements on individual multiwalled carbon nanotubes. *Phys. Rev. B* **2007**, *76*, 195436. [CrossRef]
31. Li, P.F.; Cao, K.; Jiang, C.C.; Xu, S.; Gao, L.B.; Xiao, X.F.; Lu, Y. In situ tensile fracturing of multilayer graphene nanosheets for their in-plane mechanical properties. *Nanotechnology* **2019**, *30*, 475708. [CrossRef]
32. Wang, D.S.; Chang, S.Y.; Huang, Y.C.; Wu, J.B.; Lai, H.J.; Leu, M.S. Nanoscopic observations of stress-induced formation of graphitic nanocrystallites at amorphous carbon surfaces. *Carbon* **2014**, *74*, 302–311. [CrossRef]
33. Fan, X.; Diao, D.F. The adhesion behavior of carbon coating studied by re-indentation during in situ TEM nanoindentation. *Appl. Surf. Sci.* **2016**, *362*, 49–55. [CrossRef]
34. Jacobs, T.D.B.; Ryan, K.E.; Keating, P.L.; Grierson, D.S.; Lefever, J.A.; Turner, K.T.; Harrison, J.A.; Carpick, R.W. The effect of atomic-scale roughness on the adhesion of nanoscale asperities: A combined simulation and experimental investigation. *Tribol. Lett.* **2013**, *50*, 81–93. [CrossRef]
35. Bernal, R.A.; Chen, P.; Schall, J.D.; Harrison, J.A.; Jeng, Y.R.; Carpick, R.W. Influence of chemical bonding on the variability of diamond-like carbon nanoscale adhesion. *Carbon* **2018**, *128*, 267–276. [CrossRef]
36. Lin, L.T.; Cui, T.R.; Qin, L.C.; Washburn, S. Direct measurement of the friction between and shear moduli of shells of carbon nanotubes. *Phys. Rev. Lett.* **2011**, *107*, 206101. [CrossRef]
37. Schweizer, P.; Dolle, C.; Dasler, D.; Abellan, G.; Hauke, F.; Hirsch, A.; Spiecker, E. Mechanical cleaning of graphene using in situ electron microscopy. *Nat. Commun.* **2020**, *11*, 1743. [CrossRef]
38. Hu, Z.L.; Fan, X.; Diao, D.F. Facilitation of sp^2 nanocrystallites on the formation of transfer films for stable low friction with in-situ TEM nanofriction study. *Tribol. Int.* **2022**, *174*, 107713. [CrossRef]
39. Wang, J.J.; Lockwood, A.J.; Peng, Y.; Xu, X.; Bobji, M.S.; Inkson, B.J. The formation of carbon nanostructures by in situ TEM mechanical nanoscale fatigue and fracture of carbon thin films. *Nanotechnology* **2009**, *20*, 305703. [CrossRef]
40. Casillas, G.; Liao, Y.; Jose-Yacaman, M.; Marks, L.D. Monolayer transfer layers during sliding at the atomic scale. *Tribol. Lett.* **2015**, *59*, 45. [CrossRef]
41. Bernal, R.A.; Carpick, R.W. Visualization of nanoscale wear mechanisms in ultrananocrystalline diamond by in-situ TEM tribometry. *Carbon* **2019**, *154*, 132–139. [CrossRef]
42. Kizuka, T.; Yamada, K.; Deguchi, S.; Naruse, M.; Tanaka, N. Cross-sectional time-resolved high-resolution transmission electron microscopy of atomic-scale contact and noncontact-type scannings on gold surfaces. *Phys. Rev. B-Condens. Matter* **1997**, *55*, 7398–7401. [CrossRef]
43. Haque, M.A.; Saif, M.T.A. Application of MEMS force sensors for in situ mechanical characterization of nano-scale thin films in SEM and TEM. *Sens. Actuator A-Phys.* **2002**, *97–98*, 239–245. [CrossRef]
44. Zhu, Y.; Corigliano, A.; Espinosa, H.D. A thermal actuator for nanoscale in situ microscopy testing: Design and characterization. *J. Micromech. Microeng.* **2006**, *16*, 242–253. [CrossRef]
45. Sato, T.; Tochigi, E.; Mizoguchi, T.; Ikuhara, Y.; Fujita, H. An experimental system combined with a micromachine and double-tilt TEM holder. *Microelectron. Eng.* **2016**, *164*, 43–47. [CrossRef]
46. Lu, H.H.; Wang, Z.J.; Yun, D.; Li, J.; Shan, Z.W. A new approach of using Lorentz force to study single-asperity friction inside TEM. *J. Mater. Sci. Technol.* **2021**, *84*, 43–48. [CrossRef]
47. Sato, T.; Milne, Z.B.; Nomura, M.; Sasaki, N.; Carpick, R.W.; Fujita, H. Ultrahigh strength and shear-assisted separation of sliding nanocontacts studied in situ. *Nat. Commun.* **2022**, *13*, 2551. [CrossRef]
48. He, Y.; She, D.S.; Liu, Z.Y.; Wang, X.; Zhong, L.; Wang, C.M.; Wang, G.F.; Mao, S.X. Atomistic observation on diffusion-mediated friction between single-asperity contacts. *Nat. Mater.* **2022**, *21*, 173–180. [CrossRef]
49. Haque, M.A.; Saif, M.T.A. Investigation of micro-scale materials behavior with MEMS. In Proceedings of the ASME International Mechanical Engineering Congress and Exposition, Nashville, TN, USA, 14–19 November 1999; Volume 16387, pp. 283–288.
50. Haque, M.A.; Saif, M.T.A. Microscale materials testing using MEMS actuators. *J. Microelectromech. Syst.* **2001**, *10*, 146–152. [CrossRef]
51. Haque, M.A.; Saif, M.T.A. In-situ tensile testing of nano-scale specimens in SEM and TEM. *Exp. Mech.* **2002**, *42*, 123–128. [CrossRef]
52. Zhu, Y.; Espinosa, H.D. An electromechanical material testing system for in situ electron microscopy and applications. *Proc. Natl. Acad. Sci. USA* **2005**, *102*, 14503–14508. [CrossRef]
53. Ishida, T.; Nakajima, Y.; Kakushima, K.; Mita, M.; Toshiyoshi, H.; Fujita, H. Design and fabrication of MEMS-controlled probes for studying the nano-interface under in situ TEM observation. *J. Micromech. Microeng.* **2010**, *20*, 075011. [CrossRef]
54. Sato, T.; Ishida, T.; Jalabert, L.; Fujita, H. Real-time transmission electron microscope observation of nanofriction at a single Ag asperity. *Nanotechnology* **2012**, *23*, 505701. [CrossRef]
55. Sato, T.; Jalabert, L.; Fujita, H. Development of MEMS integrated into TEM setup to monitor shear deformation, force and stress for nanotribology. *Microelectron. Eng.* **2013**, *112*, 269–272. [CrossRef]

56. Ishida, T.; Sato, T.; Ishikawa, T.; Oguma, M.; Itamura, N.; Goda, K.; Sasaki, N.; Fujita, H. Time-lapse nanoscopy of friction in the non-Amontons and non-Coulomb regime. *Nano Lett.* **2015**, *15*, 1476–1480. [CrossRef]
57. Zhang, D.F.; Breguet, J.M.; Clavel, R.; Sivakov, V.; Christiansen, S.; Michler, J. In situ electron microscopy mechanical testing of silicon nanowires using electrostatically actuated tensile stages. *J. Microelectromech. Syst.* **2010**, *19*, 663–674. [CrossRef]
58. Wang, Y.L.; Li, T.; Zhang, X.; Zeng, H.J.; Jin, Q.H. In situ TEM/SEM electronic/mechanical characterization of nano material with MEMS chip. *J. Semicond.* **2014**, *35*, 081001. [CrossRef]
59. Svensson, K.; Jompol, Y.; Olin, H.; Olsson, E. Compact design of a transmission electron microscope-scanning tunneling microscope holder with three-dimensional coarse motion. *Rev. Sci. Instrum.* **2003**, *74*, 4945–4947. [CrossRef]
60. Lockwood, A.J.; Wedekind, J.; Gay, R.S.; Bobji, M.S.; Amavasai, B.; Howarth, M.; Mobus, G.; Inkson, B.J. Advanced transmission electron microscope triboprobe with automated closed-loop nanopositioning. *Meas. Sci. Technol.* **2010**, *21*, 075901. [CrossRef]
61. Lobato-Dauzier, N.; Denoual, M.; Sato, T.; Tachikawa, S.; Jalabert, L.; Fujita, H. Current driven magnetic actuation of a MEMS silicon beam in a transmission electron microscope. *Ultramicroscopy* **2019**, *197*, 100–104. [CrossRef] [PubMed]
62. Wall, M.A.; Dahmen, U. An in situ nanoindentation specimen holder for a high voltage transmission electron microscope. *Microsc. Res. Tech.* **1998**, *42*, 248–254. [CrossRef]
63. Minor, A.M.; Morris, J.W.; Stach, E.A. Quantitative in situ nanoindentation in an electron microscope. *Appl. Phys. Lett.* **2001**, *79*, 1625–1627. [CrossRef]
64. Bobji, M.S.; Ramanujan, C.S.; Pethica, J.B.; Inkson, B.J. A miniaturized TEM nanoindenter for studying material deformation in situ. *Meas. Sci. Technol.* **2006**, *17*, 1324–1329. [CrossRef]
65. Desai, A.V.; Haque, M.A. A novel MEMS nano-tribometer for dynamic testing in-situ in SEM and TEM. *Tribol. Lett.* **2005**, *18*, 13–19. [CrossRef]
66. Erts, D.; Lohmus, A.; Lohmus, R.; Olin, H. Instrumentation of STM and AFM combined with transmission electron microscope. *Appl. Phys. A-Mater. Sci. Process.* **2001**, *72*, 71–74. [CrossRef]
67. Fujisawa, S.; Kizuka, T. Lateral displacement of an AFM tip observed by in-situ TEM/AFM combined microscopy: The effect of the friction in AFM. *Tribol. Lett.* **2003**, *15*, 163–168. [CrossRef]
68. Anantheshwara, K.; Bobji, M.S. In situ transmission electron microscope study of single asperity sliding contacts. *Tribol. Int.* **2010**, *43*, 1099–1103. [CrossRef]
69. Wang, X.; Liu, Z.Y.; He, Y.; Tan, S.S.; Wang, G.F.; Mao, S.X. Atomic-scale friction between single-asperity contacts unveiled through in situ transmission electron microscopy. *Nat. Nanotechnol.* **2022**, *17*, 799. [CrossRef]
70. Xue, P.D.; Chen, C.; Fan, X.; Diao, D.F. Current-carrying friction in carbon coated ball bearing. *Friction* **2023**, 1–13. [CrossRef]
71. Wang, X.Y.; Zhang, X.; Wang, C.; Lu, Y.; Hao, J.Y. High temperature tribology behavior of silicon and nitrogen doped hydrogenated diamond-like carbon (DLC) coatings. *Tribol. Int.* **2022**, *175*, 107845. [CrossRef]
72. Vuchkov, T.; Evaristo, M.; Carvalho, A.; Cavaleiro, A. On the tribological performance of laser-treated self-lubricating thin films in contact with rubber. *Tribol. Int.* **2022**, *174*, 107758. [CrossRef]
73. Alsem, D.H.; Sood, S.; Salmon, N.; Jacobs, T.D.B. In situ electrical testing of device-relevant nanocontacts in the transmission electron microscope. *Microsc. Microanal.* **2016**, *22*, 818–819. [CrossRef]
74. Vishnubhotla, S.B.; Chen, R.M.; Khanal, S.R.; Li, J.; Stach, E.A.; Martini, A.; Jacobs, T.D.B. Quantitative measurement of contact area and electron transport across platinum nanocontacts for scanning probe microscopy and electrical nanodevices. *Nanotechnology* **2018**, *30*, 045705. [CrossRef] [PubMed]
75. Minenkov, A.; Santic, N.; Truglas, T.; Aberl, J.; Vukusic, L.; Brehm, M.; Groiss, H. Advanced preparation of plan-view specimens on a MEMS chip for in situ TEM heating experiments. *MRS Bull.* **2022**, *47*, 359–370. [CrossRef] [PubMed]
76. Zak, A.M. Light-induced in situ transmission electron microscopy-development, challenges, and perspectives. *Nano Lett.* **2022**, *22*, 9219–9226. [CrossRef] [PubMed]
77. Tsai, P.C.; Jeng, Y.R.; Huang, Y.X.; Wu, K.T. Buckling characterizations of an individual multi-walled carbon nanotube: Insights from quantitative in situ transmission electron microscope nanoindentation and molecular dynamics. *Appl. Phys. Lett.* **2013**, *103*, 053119. [CrossRef]
78. Tsai, P.C.; Jeng, Y.R. In-situ nanomechanical study on bending characteristics of individual multi-walled carbon nanotubes. *Mater. Sci. Eng. A-Struct. Mater. Prop. Microstruct. Process.* **2016**, *658*, 389–392. [CrossRef]
79. Zhao, J.; He, M.R.; Dai, S.; Huang, J.Q.; Wei, F.; Zhu, J. TEM observations of buckling and fracture modes for compressed thick multiwall carbon nanotubes. *Carbon* **2011**, *49*, 206–213. [CrossRef]
80. Jang, B.; Kim, B.; Kim, J.H.; Lee, H.J.; Sumigawa, T.; Kitamura, T. Asynchronous cracking with dissimilar paths in multilayer graphene. *Nanoscale* **2017**, *9*, 17325–17333. [CrossRef]
81. Wei, X.L.; Xiao, S.; Li, F.X.; Tang, D.M.; Chen, Q.; Bando, Y.; Golberg, D. Comparative fracture toughness of multilayer graphenes and boronitrenes. *Nano Lett.* **2015**, *15*, 689–694. [CrossRef]
82. Wang, M.S.; Golberg, D.; Bando, Y. Tensile tests on individual single-walled carbon nanotubes: Linking nanotube strength with its defects. *Adv. Mater.* **2010**, *22*, 4071–4075. [CrossRef]
83. Filleter, T.; Bernal, R.; Li, S.; Espinosa, H.D. Ultrahigh strength and stiffness in cross-linked hierarchical carbon nanotube bundles. *Adv. Mater.* **2011**, *23*, 2855–2860. [CrossRef]
84. Cheng, Y.; Li, X.; Gao, H.W.; Wang, J.M.; Luo, G.F.; Golberg, D.; Wang, M.S. Diameter, strength and resistance tuning of double-walled carbon nanotubes in a transmission electron microscope. *Carbon* **2020**, *160*, 98–106. [CrossRef]

85. Cao, C.H.; Daly, M.; Chen, B.; Howe, J.Y.; Singh, C.V.; Filleter, T.; Sun, Y. Strengthening in graphene oxide nanosheets: Bridging the gap between interplanar and intraplanar fracture. *Nano Lett.* **2015**, *15*, 6528–6534. [CrossRef]
86. Cao, C.H.; Mukherjee, S.; Howe, J.Y.; Perovic, D.D.; Sun, Y.; Singh, C.V.; Filleter, T. Nonlinear fracture toughness measurement and crack propagation resistance of functionalized graphene multilayers. *Sci. Adv.* **2018**, *4*, eaao7202. [CrossRef]
87. Cao, C.H.; Howe, J.Y.; Perovic, D.; Filleter, T.; Sun, Y. In situ TEM tensile testing of carbon-linked graphene oxide nanosheets using a MEMS device. *Nanotechnology* **2016**, *27*, 28LT01. [CrossRef]
88. Chen, C.; Xue, P.D.; Diao, D.F. Graphitization vs tribo-oxidation governing friction behaviors of doped graphene nanocrystalline carbon films. *Carbon* **2022**, *197*, 435–443. [CrossRef]
89. Wan, N.; Pan, W.; Lin, T. Strain-induced growth of oriented graphene layers revealed by in situ transmission electron microscopy observation. *Phys. Chem. Chem. Phys.* **2016**, *18*, 16641–16646. [CrossRef]
90. Beese, A.M.; Papkov, D.; Li, S.Y.; Dzenis, Y.; Espinosa, H.D. In situ transmission electron microscope tensile testing reveals structure-property relationships in carbon nanofibers. *Carbon* **2013**, *60*, 246–253. [CrossRef]
91. Jacobs, T.D.B.; Lefever, J.A.; Carpick, R.W. A technique for the experimental determination of the length and strength of adhesive interactions between effectively rigid materials. *Tribol. Lett.* **2015**, *59*, 1. [CrossRef]
92. Jacobs, T.D.B.; Lefever, J.A.; Carpick, R.W. Measurement of the length and strength of adhesive interactions in a nanoscale silicon-diamond interface. *Adv. Mater. Interfaces* **2015**, *2*, 1400547. [CrossRef]
93. Carpick, R.W.; Bernal, R.A.; Chen, P.; Schall, J.D.; Harrison, J.A. Influence of chemical bonding on the variability of diamond-like carbon nanoscale adhesion: An in-situ TEM/nanoindentation and molecular dynamics study. *Microsc. Microanal.* **2018**, *24*, 1822–1823. [CrossRef]
94. Milne, Z.B.; Schall, J.D.; Jacobs, T.D.B.; Harrison, J.A.; Carpick, R.W. Covalent bonding and atomic-level plasticity increase adhesion in silicon-diamond nanocontacts. *ACS Appl. Mater. Interfaces* **2019**, *11*, 40734–40748. [CrossRef] [PubMed]
95. Vishnubhotla, S.B.; Chen, R.M.; Khanal, S.R.; Hu, X.L.; Martini, A.; Jacobs, T.D.B. Matching atomistic simulations and in situ experiments to investigate the mechanics of nanoscale contact. *Tribol. Lett.* **2019**, *67*, 97. [CrossRef]
96. Milne, Z.B.; Bernal, R.A.; Carpick, R.W. Sliding history-dependent adhesion of nanoscale silicon contacts revealed by in situ transmission electron microscopy. *Langmuir* **2019**, *35*, 15628–15638. [CrossRef] [PubMed]
97. Liang, J.H.; Milne, Z.; Rouhani, M.; Lin, Y.P.; Bernal, R.A.; Sato, T.; Carpick, R.W.; Jeng, Y.R. Stress-dependent adhesion and sliding-induced nanoscale wear of diamond-like carbon studied using in situ TEM nanoindentation. *Carbon* **2022**, *193*, 230–241. [CrossRef]
98. Liu, Z.; Yang, J.R.; Grey, F.; Liu, J.Z.; Liu, Y.L.; Wang, Y.B.; Yang, Y.L.; Cheng, Y.; Zheng, Q.S. Observation of microscale superlubricity in graphite. *Phys. Rev. Lett.* **2012**, *108*, 205503. [CrossRef]
99. Kis, A.; Jensen, K.; Aloni, S.; Mickelson, W.; Zettl, A. Interlayer forces and ultralow sliding friction in multiwalled carbon nanotubes. *Phys. Rev. Lett.* **2006**, *97*, 025501. [CrossRef]
100. Fan, X.; Hu, Z.L.; Huang, W.C. In-situ TEM studies on stick-slip friction characters of sp^2 nanocrystallited carbon films. *Friction* **2022**, *10*, 1635–1649. [CrossRef]
101. Sato, T.; Nabeya, S.; Menon, V.; Ishida, T.; Kometani, R.; Fujita, H. Real-time observation of slipping and rolling events in DLC wear nanoparticles. *Nanotechnology* **2018**, *29*, 325707. [CrossRef]
102. Hintsala, E.D.; Stauffer, D.D.; Oh, Y.; Asif, S.A.S. In situ TEM scratch testing of perpendicular magnetic recording multilayers with a novel MEMS tribometer. *JOM* **2017**, *69*, 51–56. [CrossRef]
103. Liu, J.J.; Jiang, Y.J.; Grierson, D.S.; Sridharan, K.; Shao, Y.C.; Jacobs, T.D.B.; Falk, M.L.; Carpick, R.W.; Turner, K.T. Tribochemical wear of diamond-like carbon-coated atomic force microscope tips. *ACS Appl. Mater. Interfaces* **2017**, *9*, 35341–35348. [CrossRef]
104. Merkle, A.P.; Erdemir, A.; Eryilmaz, O.L.; Johnson, J.A.; Marks, L.D. In situ TEM studies of tribo-induced bonding modifications in near-frictionless carbon films. *Carbon* **2010**, *48*, 587–591. [CrossRef]
105. M'ndange-Pfupfu, A.; Eryilmaz, O.; Erdemir, A.; Marks, L.D. Quantification of sliding-induced phase transformation in N3FC diamond-like carbon films. *Diam. Relat. Mat.* **2011**, *20*, 1143–1148. [CrossRef]
106. Johnson, J.A.; Holland, D.; Woodford, J.B.; Zinovev, A.; Gee, I.A.; Eryilmaz, O.L.; Erdemir, A. Top-surface characterization of a near frictionless carbon film. *Diam. Relat. Mat.* **2007**, *16*, 209–215. [CrossRef]
107. M'ndange-Pfupfu, A.; Ciston, J.; Eryilmaz, O.; Erdemir, A.; Marks, L.D. Direct observation of tribochemically assisted wear on diamond-like carbon thin films. *Tribol. Lett.* **2013**, *49*, 351–356. [CrossRef]
108. Eryilmaz, O.L.; Erdemir, A. Surface analytical investigation of nearly-frictionless carbon films after tests in dry and humid nitrogen. *Surf. Coat. Technol.* **2007**, *201*, 7401–7407. [CrossRef]
109. Merkle, A.P.; Marks, L.D. Friction in full view. *Appl. Phys. Lett.* **2007**, *90*, 064101. [CrossRef]